Gel formation in a mixture of a block copolymer and a nematic liquid crystal

Maxim Khazimullin,[*] Thomas Müller, Stephan Messlinger, Ingo Rehberg, and Wolfgang Schöpf[†]
Experimentalphysik V, Universität Bayreuth, DE-95440 Bayreuth, Germany

Alexei Krekhov[‡]
Theoretische Physik I, Universität Bayreuth, DE-95440 Bayreuth, Germany

Robin Pettau, Klaus Kreger, and Hans-Werner Schmidt[§]
Makromolekulare Chemie I, Universität Bayreuth, DE-95440 Bayreuth, Germany
(Received 14 March 2011; published 29 August 2011)

The viscoelastic properties of a binary mixture of a mesogenic side-chain block copolymer in a low molecular weight nematic liquid crystal are studied for mass concentrations ranging from the diluted regime up to a liquid crystalline gel state at about 3%. In the gel state, the system does not flow, exhibits a polydomain structure on a microscopic level, and strongly scatters light. Below the gelation point, the system is homogeneous and behaves like a usual nematic, so the continuum theory of liquid crystals can be applied for interpreting the experimental data. Using the dynamic Fréedericksz transition technique, the dependence of the splay elastic constant and the rotational viscosity on the polymer concentration have been obtained. Comparing the dynamic behavior of block copolymer solutions with the respective homopolymer solutions reveals that, above a mass concentration of 1%, self-assembling of the block copolymer chain segments in clusters occurred, resulting in a gel state at higher concentrations. The effective cluster size is estimated as a function of the concentration, and a scaling-law behavior near the sol-gel transition is confirmed. This technique may serve as an alternative method for determining the gelation point.

DOI: 10.1103/PhysRevE.84.021710 PACS number(s): 42.70.Df, 83.80.Kn, 64.70.mj, 82.70.Gg

I. INTRODUCTION

Gels are systems that consist of at least two components: the minor component forms an elastic network (e.g., by means of cross-linked polymer molecules), which prevents the major component, a liquid, from flowing out [1,2]. As a consequence, a gel is solid in the sense that it keeps its shape, but is easily deformed by mechanical forces. Liquid crystals are anisotropic fluids with a long-range orientational order, resulting in a very sensitive response to external fields [3]. Using a low molecular weight liquid crystal as a solvent, liquid crystalline gels can be prepared that combine the soft-solid nature of the gel with the anisotropy of the liquid crystal [4,5]. Due to the weak resistance of the gelator network to mechanical forces and the high susceptibility of liquid crystals to external fields, the shape of the liquid crystalline gel can be easily changed by a low electrical voltage [6,7], thus permitting the creation of microactuators or artificial muscles [8]. It has been shown recently that, in a liquid crystalline gel, the electro-optical response can be fast due to the elastic interaction between the liquid crystal and the network [9]. Because of the polydomain structure forming in nonaligned liquid crystalline gels, such displays can be operated in scattering mode and, thus, do not require polarizers. From a fundamental point of view, one of the most interesting issues in these gels is the consequence of the coupling between the elastic network and the liquid crystal ordering.

Liquid crystalline gels can be prepared in different ways by mixing low molecular compounds or various polymers (gelators) with a liquid crystal. In chemical gels, an extended network is formed due to chemical or photochemical reactions between the gelator molecules [4,10]. A typical feature of such a system is irreversibility: once formed, the network can not be destroyed easily. In a physical gel, on the other hand, the network is formed due to intermolecular interactions between the gelator molecules that lead to the thermoreversibility of the physical cross links in the network. The physical properties of such systems can be changed relatively easily, e.g., by temperature, which makes them attractive for the study and the implementation of new device operation principles [4].

An interesting approach is the creation of physical liquid crystalline gels where triblock copolymers are used as a gelator [9,11]. The block copolymers consist of a middle block with attached liquid crystal mesogenes so that it is miscible with a liquid crystal, and of end blocks that are well soluble in the isotropic phase but not in the nematic phase of the solvent. Due to microphase separation, the end blocks are aggregating in the nematic solvent, creating the nodes of a supramolecular network. By heating the gel above the nematic-isotropic transition temperature (the clearing point), the network is disassembled, showing the reversible nature of the system [9,12]. Such gels typically form a polydomain structure at room temperature that scatters light intensively. It is also possible to create monodomain samples by shearing or by applying a strong magnetic field while cooling the

[*]Permanent address: Institute of Physics of Molecules and Crystals of the Ufa Scientific Center, Russian Academy of Science, Ufa, Russia.
[†]wolfgang.schoepf@uni-bayreuth.de
[‡]alexei.krekhov@uni-bayreuth.de
[§]hans-werner.schmidt@uni-bayreuth.de

sample down from the isotropic state [9]. The peculiarities of the rheological behavior near the clearing point have been attributed to changes in the network structure of the liquid crystalline gel and are not yet fully understood [12]. Dynamic light scattering shows two different time scales [13]: a fast scale that has been related to the orientational relaxation and a slow scale arising from the network rearrangement process.

While the investigations of the viscoelastic and optical properties of physical liquid crystalline gels are currently only at the beginning, much more effort has been invested to understand the structure of individual polymer chains and the dynamic properties of dilute solutions of various polymers in nematic solvents [14]. The main feature is that the conformation of a single polymer chain in a nematic environment is anisotropic [15–17]. The shape of the polymer chain strongly depends on the chemical structure of the polymer and also changes with temperature [9,14,18–20]. Typically, main-chain polymers, where mesogenes are part of the backbone, develop a strong prolate conformation with the long axes being parallel to the nematic director [14]. For a side-chain polymer, a prolate conformation is observed for side-on attachment and an oblate conformation for end-on attachment of the mesogenic units [9,21].

The flow properties of polymer solutions in nematics are characterized by an anisotropic viscous tensor, with the viscosity coefficients strongly depending on the chain conformation leading to remarkable effects. In particular, the addition of liquid crystalline side-chain polymers to a vertically aligned liquid crystal reduces the backflow effect, which arises during the director reorientation and is undesirable in displays [18]. Depending on the viscosity coefficients, nematic liquid crystals are oriented at a certain angle relative to the direction of the flow, so-called flow-aligning nematics, or show a tumbling behavior. The addition of a main-chain polymer with a prolate conformation changes the rheology from a tumbling behavior to a flow-aligning behavior [22]. The opposite effect is observed when using a side-chain polymer with oblate chain shape [22,23].

Despite numerous studies of a polymer dissolved in a liquid crystal, most of them were done in diluted solutions, or for polymers that do not form a liquid crystalline gel [14]. In this paper, we study the transition from the diluted regime to the gel state of triblock copolymer solutions in a nematic liquid crystal by varying the polymer concentration. We use the Fréedericksz transition technique, which is based on the optical detection of the reorientation of the liquid crystal in an electric field [24,25]. The optical response to a slowly changing electric field allows us to study the elastic properties, while switching the field on and off yields information about the viscous properties. Previously, this technique has been successfully applied to investigate dilute solutions of a polymer in a liquid crystal [18,26] and to liquid crystalline gels [27–29]. Our results on the orientational dynamics of the block copolymer solutions approaching the gel point allow to identify the self-assembling of individual chains in clusters. Based on the Brochard model [15], we find a scaling-law behavior of the cluster sizes as well as the critical concentration for the sol-gel transition.

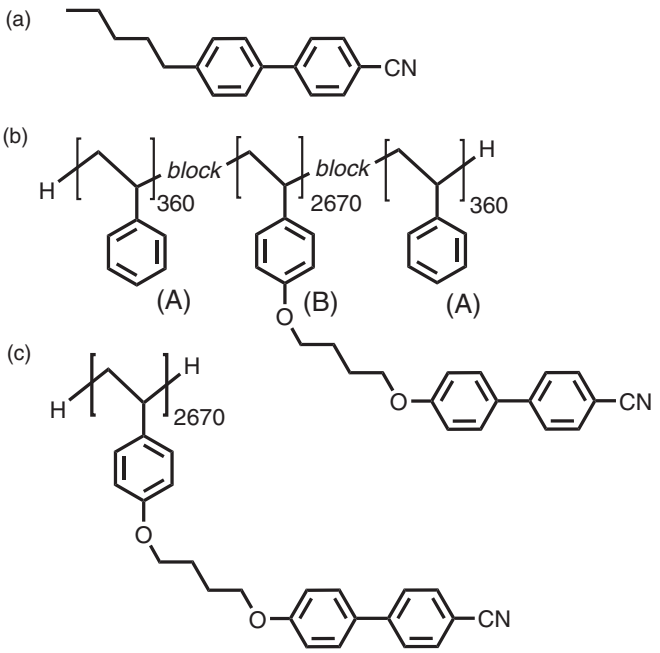

FIG. 1. (a) Nematic liquid crystal 4-Cyano-(4′-pentyl)biphenyl, 5CB. (b) Cyanobiphenyl functionalized block copolymer. (c) Corresponding homopolymer. The average number of repeating units of each segment is given.

II. SAMPLE PREPARATION AND EXPERIMENTAL SETUP

A. Sample preparation

We use the low molecular weight liquid crystal 4-cyano-(4′-pentyl)biphenyl [5CB; see Fig. 1(a)], which is commercially available from abcr GmbH. 5CB is nematic at room temperature with a nematic-isotropic transition (clearing point) at 35 °C.

The chemical structure of the mesogenic side-chain block copolymer (MSCBCP) used for our mixtures is shown in Fig. 1(b). This block copolymer was specifically designed to act as a gelator for low molecular weight liquid crystals. To achieve this, the middle block (B) was functionalized with moieties that are structurally similar to 5CB so that this segment is soluble in the isotropic and in the nematic phase of 5CB. In contrast, the polystyrene end blocks (A) of the MSCBCP are insoluble in the nematic phase but soluble in the isotropic phase of 5CB. Dissolution of the end blocks in a nematic solvent is unfavorable because it drastically decreases the enthalpy of the dissolved polymer. Upon cooling below the clearing temperature, the middle block remains dissolved, whereas the end blocks phase separate from the nematic solvent. Above a critical block copolymer concentration, a physical network is formed when the end blocks of different block copolymer chains self-assemble and form the nodes of the network [9].

This ABA-triblock copolymer comprises a poly(4-hydroxystyrene) middle block (B) functionalized with 4-cyanobiphenyl moieties, which is covalently linked to polystyrene end blocks (A) and was prepared by a polymer-analogous approach [30–33]. The polymer backbone was prepared by sequential anionic polymerization of 4-tert-butoxystyrene and styrene in tetrahydrofuran with sodium naphthalene as initiator. Prior to the polymer-analogous

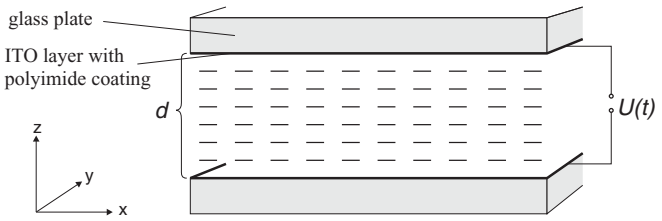

FIG. 2. Sketch of the liquid crystal cell and definition of the coordinate system.

functionalization, the tert-butoxy protection group was removed by acidic cleavage. 4-(4-bromobutoxy)-4′-cyanobiphenyl moieties, which were prepared separately, were subsequently attached to the middle block in a polymer-analogous etherification reaction. The degree of conversion of the polymer-analogous reaction was determined by ^{1}H-NMR to 84%. The molecular weight was analyzed by size exclusion chromatography (SEC). The number-average molecular weight M_n of the MSCBCP was determined to 1560 kg/mol with a polydispersity index of 1.29. The repeating units were determined from the results of ^{1}H-NMR and SEC from the precursor polymer to be 360 in the A block and 2670 in the B block. Details regarding the synthesis and characterization of the block copolymer and of the respective homopolymer (see below) can be found in the Supplemental Material [34].

Mixtures of the block copolymer and 5CB were prepared by weighing the solvent and the respective amount of polymer in a 1.5-mL vial. The closed vial was placed in a tumble mixer at a temperature of 50 °C for three days to ensure homogeneous mixing. For our experiments, mixtures with block copolymer mass concentrations c ranging from 0.2% to 5% have been used. Rheology measurements revealed that the critical mass concentration of the block copolymer, at which the system is gelified, is around 3% [35].

For the dynamic and static measurements, the different MSCBCP-5CB mixtures were filled into commercially available liquid crystal cells (see Fig. 2 for a sketch).[1] They consist of two parallel, transparent electrodes [glass plates with an indium tin oxide (ITO) layer on the inside], which are separated by spacers. The ITO surfaces of the electrodes are coated with polyimide and rubbed in one direction in order to produce a planar alignment. When this probe is filled with a nematic material, the director is aligned along the rubbing direction in the layer plane. This direction defines the x axis, with the y axis being perpendicular to x in the layer plane. The thickness d of the cell is determined by the spacer that separates the two glass plates in the z direction. We have measured the thickness with an accuracy of $\pm 0.5\ \mu$m, using an interferometric method [36]. For the cells we used, the typical thickness was about 27.5 μm.

Before filling the cells, the mixtures were heated to and kept at a temperature of 60 °C for 2 h. Then, the isotropic solution was filled into the cell by capillary forces. In order to remove concentration gradients that may have formed inside the cell during filling, the system was kept at this temperature for another 2 h and was allowed to cool to the ambient temperature within 12 h. For block copolymer mass concentrations below 2.5%, the samples were homogeneously aligned directly after filling [Fig. 3(a)]. Above 2.5%, some misaligning of the liquid crystal layer has occurred [Fig. 3(b)], but after keeping the samples for a few weeks at room temperature, monodomain samples were observed. For a block copolymer mass concentration of 5%, the gel network has already formed, therefore, the sample images exhibit a polydomain texture, even after keeping it for several weeks at room temperature [Fig. 3(c)].

To compare the results of the 5CB-block copolymer mixtures with liquid crystal-polymer mixtures where no self-assembly of polystyrene end blocks can occur, we also prepared the respective mesogenic side-chain homopolymer of the middle block of the above-described triblock copolymer. The homopolymer has the same chemical structure as the block copolymer, but without the polystyrene end blocks (A) [see Fig. 1(c)]. The number-average molecular weight was determined to be $M_n = 1637$ kg/mol with a polydispersity index of 1.16. The degree of conversion was 97%. Solutions of the homopolymer in 5CB were prepared in similar concentrations as for the block copolymer. The mixing and filling procedures were performed in the same manner as described above. Due to the missing end blocks, no gel is formed in the homopolymer solutions.

B. Experimental setup

We use the standard experimental setup as described, e.g., in Refs. [37,38] and sketched in Fig. 4. An ac voltage $U(t) = U_{\rm rms}\sqrt{2}\cos(2\pi f t)$ was applied across the cell by means of a waveform generator (Agilent Technologies, 33220A) and an amplifier with a maximum output voltage $U_{\rm rms} = 120$ V. The voltage at the liquid crystal cell was measured by a digital multimeter (Prema, 5017 DMM) and the frequency was kept constant at $f = 1$ kHz for all measurements. The cell was mounted on a thermostage. The temperature of the cell was kept constant at $T = (25.0 \pm 0.2)$ °C by means of a circulation thermostat (Lauda, RE305) and was measured with a PT100 platinum temperature sensor with an accuracy of ± 0.1 K. The thermostage was fixed to a polarizing microscope (Olympus, BX41). All measurements were done between crossed polarizers. As a light source, a red LED (LedEngin, LZ4-00R115, wavelength $\lambda = 638$ nm) was used.

The microscopic images of the samples were captured by a digital USB camera (Lumenera Corporation, LU135M-IO) that has a spatial resolution of 1280 × 1024 pixels and 256 gray scales. The time intervals between images were provided by a high-precision pulse generator. Depending on the sampling speed, resolutions ranging from 128 × 128 pixels for the fastest experiments to the full range for slower experiments have been used. The sampling rate was in the range between 0.1 and 25 Hz, depending on the respective experiment. From the acquired images, the transmitted light intensity was determined in different areas of the sample. The experimental setup allows us to measure the dependence of the light intensity on the applied voltage (static measurements) as well as the temporal evolution of the light intensity (dynamic measurements).

[1] E.H.C. Co. Ltd., 1164 Hino, Hino-shi, Tokyo, Japan 191.

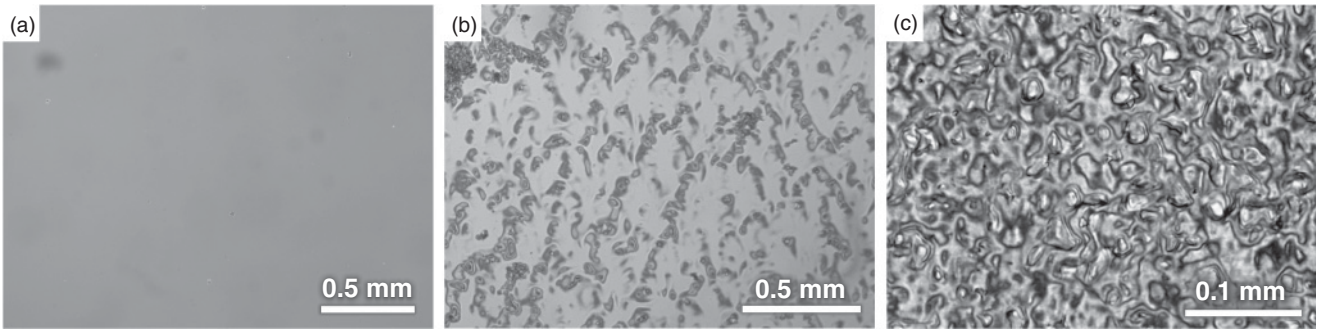

FIG. 3. Images of cells filled with samples of different concentrations c of the block copolymer taken between crossed polarizers. (a) $c = 1.1\%$; (b) $c = 3.0\%$; (c) $c = 5.0\%$. Note the different scales.

For measuring the dielectric anisotropy ϵ_a of the polymer solutions in the liquid crystal, we used a conductivity lock-in amplifier to determine the capacities of the cells as, for example, described in Ref. [39]. ϵ_a can then be calculated by $\epsilon_a = \frac{C_\parallel - C_\perp}{C_0}$, where $C_\perp$ is the capacity of the cell measured at a small ac voltage well below the Fréedericksz threshold, $C_\parallel$ is the extrapolated limit of the capacity for high voltages, and C_0 is the capacity of the empty cell.

III. STATIC MEASUREMENTS

A. Birefringence method

The measurement of the critical Fréedericksz voltage U_F is well suited to determine the elasticity in our system, as U_F is determined by the dielectric anisotropy ϵ_a and by the splay elastic constant k_{11} [40,41]:

$$U_F = \pi \sqrt{\frac{k_{11}}{\epsilon_0 \epsilon_a}}. \tag{1}$$

Thus, from the measurements of U_F and ϵ_a, we can detect the influence of the polymer concentration on the elasticity.

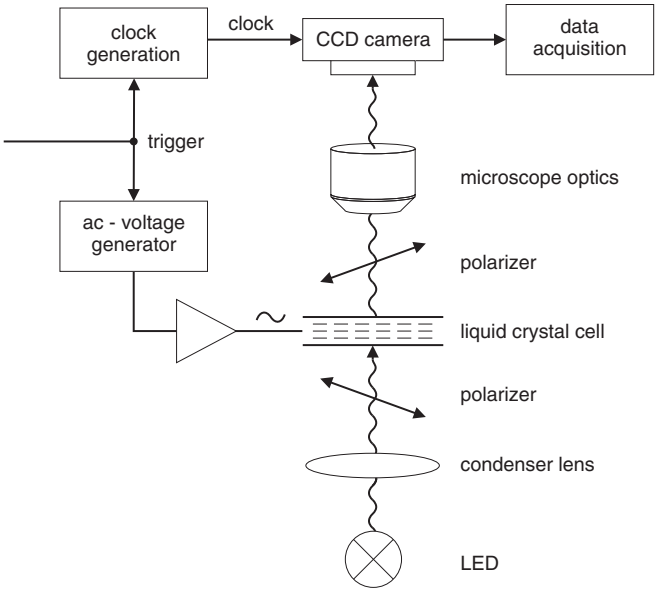

FIG. 4. Sketch of the experimental setup.

For determining the Fréedericksz threshold, we use the birefringence technique [25,41]. The refractive index of a nematic liquid crystal is anisotropic with $n_\perp$ being the refractive index for light polarized perpendicular to the nematic director and $n_\parallel$ for light polarized along the director. The refractive index for the ordinary light ray n_o is always given by $n_o = n_\perp$, even if the director deviates from the original orientation along the x axis, as long as it remains perpendicular to the y axis. The refractive index for the extraordinary light ray n_e, however, depends on the director angle θ, i.e., the angle between the director and the x axis. If θ varies along the z axis, n_e depends on the vertical location inside the cell:

$$n_e = \frac{n_\perp n_\parallel}{\sqrt{n_\perp^2 \cos^2\theta(z) + n_\parallel^2 \sin^2\theta(z)}}, \quad n_o = n_\perp. \tag{2}$$

The birefringence $\Delta n = n_e - n_o$ is 0 for a homeotropic director orientation ($\theta = \frac{\pi}{2}$) and maximal at $n_a = n_\parallel - n_\perp$ for the initial planar orientation ($\theta = 0$). The birefringence leads to a phase difference δ between the ordinary and the extraordinary ray, where δ is found by integrating Δn over the layer height d:

$$\delta = \frac{2\pi}{\lambda} \int_0^d \{n_e[\theta(z)] - n_o\}\, dz. \tag{3}$$

In our experimental procedure, we can determine δ from measuring the transmitted light intensity I as a function of the applied voltage U_{rms}, and subsequently the critical voltage U_F from $\delta(U_{rms})$, as shown in the following.

By using the setup described in Sec. II B with crossed polarizers and an angle of 45° between the polarizers and the x direction, the ordinary and the extraordinary rays are brought to interference. Thus, the intensity of the transmitted light is ideally given by $I = I_0 \sin^2 \frac{\delta}{2}$, when I_0 is the maximally transmitted light intensity. In the experiment, we rather observe

$$I(U_{rms}) = I_b + I_0 \sin^2 \frac{\delta(U_{rms})}{2} \tag{4}$$

for a certain voltage U_{rms} above the Fréedericksz transition. I_b is an intensity offset due to stray light and other influences and has to be extracted from the experimental data. Below the Fréedericksz transition, corresponding to the homogeneous planar orientation ($\theta = 0$), the measured intensity $I(U_{rms})$ is

constant and δ is given by the maximal phase difference $\delta_0 = \delta(U_{\rm rms} < U_{\rm F})$ with

$$\delta_0 = \frac{2\pi d}{\lambda}(n_\parallel - n_\perp) = \frac{2\pi d}{\lambda} n_{\rm a}. \tag{5}$$

The minimal phase difference of $\delta = 0$ is reached when the liquid crystal layer is almost homeotropically aligned, i.e., for very high voltages ($U_{\rm rms} \approx 120$ V in our case). Between these two extrema, the light intensity undergoes a number of minima and maxima, depending on the value of δ_0 and thus on d, λ, and $n_{\rm a}$. In order to extract δ and thus δ_0 from the experiment, Eq. (4) has to be inverted, which can only be done piecewise, starting from $\delta = 0$:

$$\delta = 2\pi M + (-1)^N \times 2 \arcsin \sqrt{\frac{I - I_{\rm b}}{I_0}}. \tag{6}$$

N is the number of intensity extrema and M the number of intensity maxima already encountered. $I_{\rm b}$ is determined by the nearest minimum and I_0 by the difference between the nearest extrema. Below the Fréedericksz transition, δ remains constant at δ_0.

The phase difference δ is determined by the director field $\theta(z)$ inside the cell [see Eq. (3)]. Obviously, Eq. (3) can not be inverted, so that $\theta(z)$ can not be determined unambiguously from δ. However, assuming a harmonic director profile slightly above the Fréedericksz transition (see, e.g., Ref. [3]), $\theta(z) = \theta_{\rm m} \sin(\pi \frac{z}{d})$, where $\theta_{\rm m}$ is the director deflection in the middle of the cell, one finds

$$\delta(\theta_{\rm m}) = \delta_0 - \delta_2 \theta_{\rm m}^2 + O\left(\theta_{\rm m}^4\right) \quad \text{with} \quad \delta_2 = \frac{\pi d}{2\lambda}\left(\frac{n_\parallel^3}{n_\perp^2} - n_\parallel\right). \tag{7}$$

Inserting the stationary overcritical director amplitude

$$\theta_{\rm m}(U_{\rm rms}) \propto \sqrt{\frac{U_{\rm rms} - U_{\rm F}}{U_{\rm F}}}, \tag{8}$$

as resulting from the pitchfork bifurcation behavior near the Fréedericksz transition [see Eq. (11) below], we expect the supercritical phase difference to decrease linearly from δ_0:

$$\frac{\delta(U_{\rm rms})}{\delta_0} - 1 \propto U_{\rm F} - U_{\rm rms}, \tag{9}$$

so that $U_{\rm F}$ is given by the point, were δ deviates from the constant value δ_0.

B. Results

In order to calculate δ, the intensities have been measured up to $U_{\rm rms} = 120$ V, where the samples are almost homeotropic with $\delta \approx 0$. We can find δ and thus δ_0 by using Eq. (6). We will use δ_0, which for our cells is found to be around $\delta_0 \approx 49$ rad, for normalization purposes, so that we can compare the results for different samples. Slightly above the Fréedericksz transition, the orientation of the director changes very slowly so that quasistatic measurements can only be done with very long waiting times between the voltage changes. Figure 5 shows the phase difference δ, normalized by the respective δ_0, as a function of the applied voltage near the critical point $U_{\rm F}$ for pure 5CB and for the block copolymer solution with a mass concentration of 1.1% for different waiting times. For pure 5CB, we find $U_{\rm F}^{\rm 5CB} = 0.73$ V, and the Fréedericksz transition leads to a sharp linear decrease of δ as described by Eq. (9). This indicates that the cells provide a planar alignment with no or very small pretilt, which is also confirmed by the observation of domain walls in the sample during the transition.

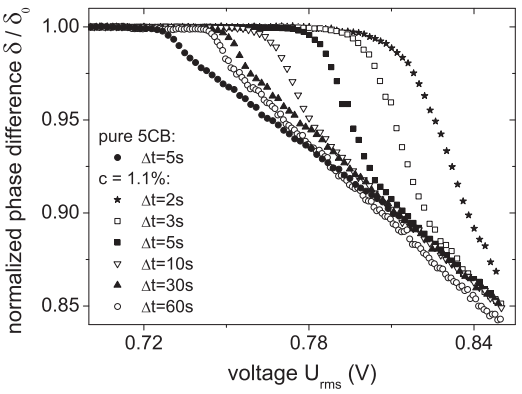

FIG. 5. Voltage dependence of the optical phase difference near the Fréedericksz transition for pure 5CB and for the block copolymer solution with a mass concentration of 1.1%. The voltage steps are always $\Delta U = 2$ mV with different time delays Δt between the voltage steps.

For the block copolymer solutions, we commonly observe an inhomogeneous Fréedericksz transition, which again we believe is due to domains of opposing director elongations forming in the nonpretilt cells. After switching off the voltage, the samples relax back to the initial state, so that the results can be reproduced. We have used different delay times between the voltage steps of $\Delta U = 2$ mV, varying from $\Delta t = 2$ to 60 s. With increasing delay time, the deviation from the horizontal line $\delta/\delta_0 = 1$ occurs for smaller voltages, misleadingly indicating a successively lower critical value. Even for the largest delay time, we could not reach the same critical value $U_{\rm F}$ as for pure 5CB, although we will show later in Sec. IV B that the thresholds indeed coincide. It should be noted that, for pure 5CB, all measurement curves coincide already for $\Delta t = 3$ s.

A further increase of the block copolymer concentration leads to prohibitively long waiting times, so that this static method is not convenient for the determination of $U_{\rm F}$ for our polymer solutions. Nevertheless, we will use the extraction of the phase difference δ for the dynamical measurements described in the next section.

IV. DYNAMICAL MEASUREMENTS

A. Method

By performing dynamical measurements, we can derive the influence of the polymers on the elasticity and on the viscosity of the system. If the applied electrical field is suddenly changed to or from an overcritical voltage $U > U_{\rm F}$, the director field will reorient with a characteristic time scale. We consider two processes: changing the voltage from a value below the critical point $U_{\rm F}$ to a target value $U_{\rm on}$ slightly above $U_{\rm F}$ (the "on" process); and switching the voltage off from a supercritical value (the "off" process).

The orientational behavior near the onset of the Fréedericksz transition is described in the framework of a weakly nonlinear analysis of the nematohydrodynamic equations [3]. For small distortions from the planar ground state, the deformation of the nematic director can be approximated by a single harmonic mode

$$\theta(z,t) = \theta_{\mathrm{m}}(t)\sin\left(\frac{\pi z}{d}\right). \tag{10}$$

Up to third order in θ_{m}, the resulting dynamic equation for the director amplitude then takes the form [25]

$$\tau_0 \frac{\partial \theta_{\mathrm{m}}}{\partial t} = \varepsilon\theta_{\mathrm{m}} - \beta\theta_{\mathrm{m}}^3, \tag{11}$$

where

$$\tau_0 = \frac{d^2\gamma_1}{k_{11}\pi^2} \tag{12}$$

is the director relaxation time, $\varepsilon = U^2/U_{\mathrm{F}}^2 - 1$ is the reduced driving voltage, and β is the saturation parameter that determines the final supercritical director amplitude. For the interpretation of our results, the value of β is not important. The director relaxation time τ_0 depends on the rotational viscosity γ_1. When taking into account the backflow effect, γ_1 should be replaced by $\gamma_1 - \alpha_3^2/\eta$, where $\eta = (\alpha_3 + \alpha_4 + \alpha_6)/2$ and α_i are the Leslie viscosity coefficients. For typical rod-shaped nematics $\alpha_3^2/(\eta\gamma_1) \approx 10^{-3}$, so that the correction to γ_1 can be neglected [25].

For subcritical voltages ($\varepsilon < 0$), all deformations of the director relax to the planar ground state $\theta_{\mathrm{m}} = 0$. For supercritical voltages ($\varepsilon > 0$), the planar state becomes unstable, so that any initial fluctuation θ_{i} will grow exponentially in time. Caused by the nonlinear term in Eq. (11), the growth will eventually saturate to the stable equilibrium value $\theta_{\mathrm{f}} = \pm\sqrt{\varepsilon/\beta}$, where the sign is determined by the direction of the initial deformation. Note that, in all practical situations, there will always be a small initial deviation from the ideal director alignment along x due to thermal fluctuations.

The saturation behavior of the "on" process is described by the solution of Eq. (11):

$$\theta_{\mathrm{on}}^2(t) = \frac{\theta_{\mathrm{f}}^2}{1 + \left(\theta_{\mathrm{f}}^2/\theta_{\mathrm{i}}^2 - 1\right)e^{-2t/\tau_{\mathrm{on}}}} \quad \text{with} \quad \tau_{\mathrm{on}} = \frac{\tau_0}{\varepsilon}. \tag{13}$$

For the "off" process ($\varepsilon = -1$), the nonlinear term in Eq. (11) can be neglected, leading to a simple exponential decay

$$\theta_{\mathrm{off}}(t) = \theta_{\mathrm{f}} e^{-t/\tau_{\mathrm{off}}} \quad \text{with} \quad \tau_{\mathrm{off}} = \tau_0. \tag{14}$$

The combination of τ_{on} and τ_{off} yields the material parameters of the nematic. From $\tau_{\mathrm{off}}/\tau_{\mathrm{on}} = \varepsilon = U_{\mathrm{on}}^2/U_{\mathrm{F}}^2 - 1$, we find the critical Fréedericksz voltage U_{F} as

$$U_{\mathrm{F}} = \frac{U_{\mathrm{on}}}{\sqrt{\tau_{\mathrm{off}}/\tau_{\mathrm{on}} + 1}}, \tag{15}$$

and the splay elastic constant and rotational viscosity as

$$k_{11} = \frac{\epsilon_0\epsilon_{\mathrm{a}}}{\pi^2}U_{\mathrm{F}}^2 = \frac{\epsilon_0\epsilon_{\mathrm{a}}}{\pi^2}\frac{U_{\mathrm{on}}^2}{\tau_{\mathrm{off}}/\tau_{\mathrm{on}} + 1}, \tag{16}$$

$$\gamma_1 = \frac{\pi^2}{d^2}k_{11}\tau_{\mathrm{off}} = \frac{\epsilon_0\epsilon_{\mathrm{a}}}{d^2}\frac{\tau_{\mathrm{off}}\,\tau_{\mathrm{on}}}{\tau_{\mathrm{off}} + \tau_{\mathrm{on}}}U_{\mathrm{on}}^2. \tag{17}$$

The optical response of the sample with respect to the birefringence method has already been derived in Sec. III A. Inserting Eqs. (13) and (14) into Eq. (7), we find for the time dependence of the phase difference during the switching process

$$\delta_{\mathrm{on}} = \delta_0 - \frac{D}{1 + Ce^{-2t/\tau_{\mathrm{on}}}}, \tag{18}$$

$$\delta_{\mathrm{off}} = \delta_0 - De^{-2t/\tau_{\mathrm{off}}}. \tag{19}$$

Here, $D = \delta_2\theta_{\mathrm{f}}^2$ is the total change of the phase difference and $C = \theta_{\mathrm{f}}^2/\theta_{\mathrm{i}}^2 - 1$. By fitting Eqs. (18) and (19) to the measured data, the time constants τ_{on} and τ_{off} can be determined.

B. Results

In order to measure the transmittance of the samples after a sudden voltage switch, images were captured at well defined time intervals and the light intensity was calculated from the gray levels of the images. Due to the spatially inhomogeneous transition, the intensity was analyzed at 1000 random locations for each time step. In order to reduce noise, the intensity at each location was averaged over an area of 3×3 pixels, which is much smaller than the typical size of the domains observed. Typical time dependencies of the transmitted light intensity $I(t)$ and the resulting phase difference $\delta(t)$ at one such location are shown in Fig. 6 for pure 5CB and for samples with a concentration of the block copolymer of 1.1% and 2.1%. The voltage has been switched from a subcritical to a slightly supercritical value between $U_{\mathrm{on}} = 0.85$ and 1 V, depending on the time scale of the experiment. We show here the phase

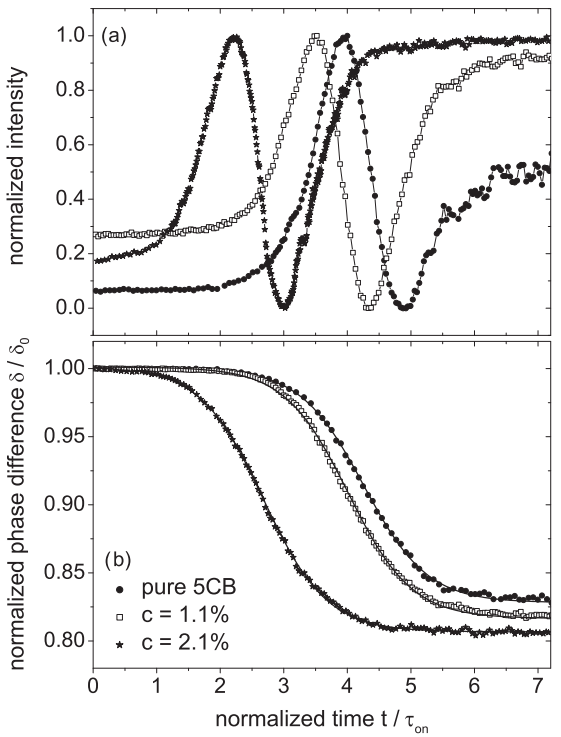

FIG. 6. Typical time dependencies of (a) the transmitted light intensity I and (b) the phase difference δ for pure 5CB and for samples with block copolymer concentrations of 1.1% and of 2.1%. The solid lines in (b) are fits of Eq. (18) to the experimental data.

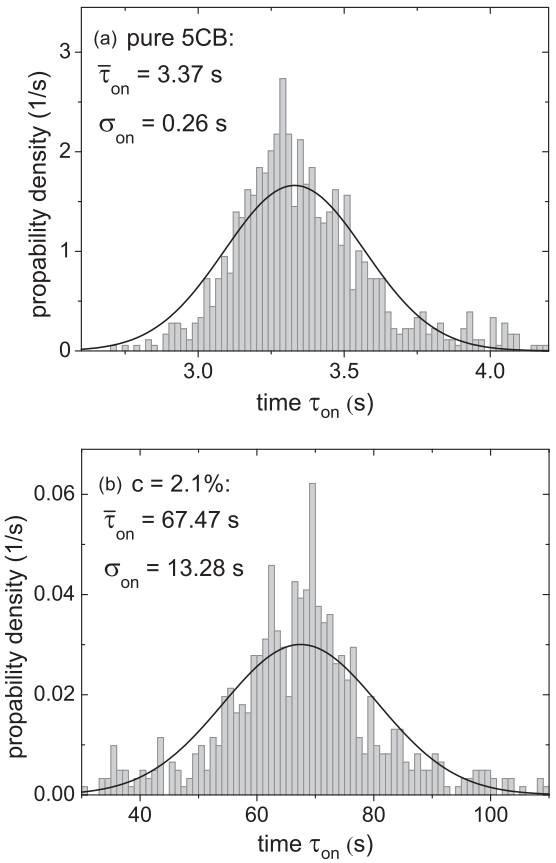

FIG. 7. Histograms of the τ_{on} distribution over the sample area (a) for pure 5CB and (b) for a block copolymer concentration of 2.1%. $\bar{\tau}_{on}$ is the mean value obtained from fitting a normal distribution (solid line) and σ_{on} is the respective standard deviation.

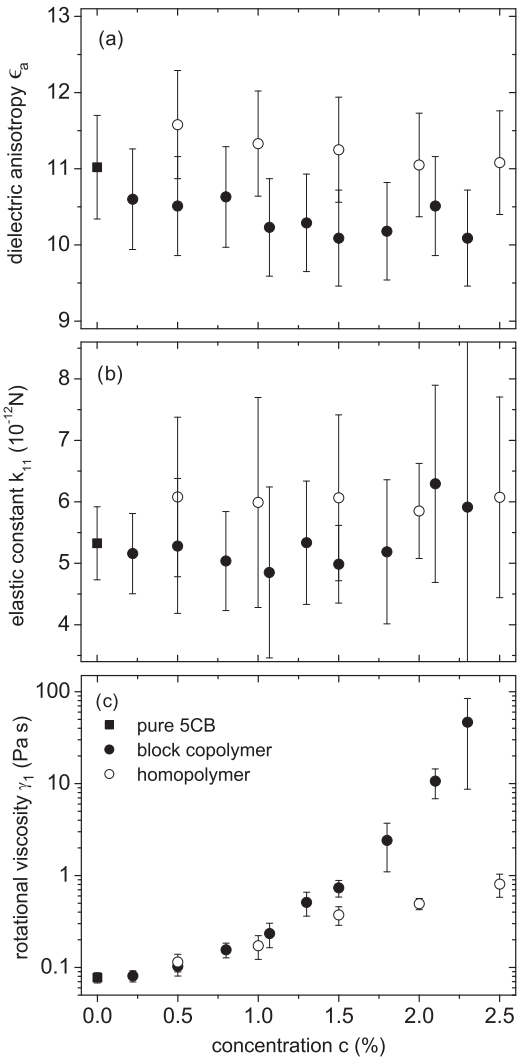

FIG. 8. As functions of the polymer concentration c are shown (a) the dielectric anisotropy ϵ_a, (b) the splay elastic constant k_{11}, and (c) the rotational viscosity γ_1. In (b) and (c) and in the following figures, the vertical bars represent the distribution of the values within our samples.

difference normalized with the value corresponding to the undistorted planar state δ_0 in order to avoid different starting levels of the curves due to slightly different cell thicknesses. The solid lines are obtained by using a nonlinear fitting procedure for Eq. (18), thus yielding τ_{on} as a fit parameter. In a similar procedure, Eq. (19) was fitted to the data obtained when switching off the voltage from a supercritical value, which gives τ_{off}.

For each of the 1000 areas, the phase difference was calculated and fitted as just explained, so that τ_{on} and τ_{off} were obtained for each small area of the sample. From histograms of these data, the mean value and its standard deviation was derived by fitting a normal distribution. Typical distributions of the "on" times τ_{on} are shown in Fig. 7(a) for pure 5CB and in Fig. 7(b) for a block copolymer solution with $c = 2.1\%$. The solid lines are fits of a normal distribution, which is typical for all our samples. It should be noted that for the "off" process, the distribution is narrower, while increasing the polymer concentration leads to a wider distribution. Since we can not assess the statistical independence of the sample areas chosen for evaluation, we characterize the uncertainties of the averaged time constants by twice the corresponding standard deviation. Thus, the bars in the following figures [except Fig. 8(a)] are not usual error bars but rather a measure for the distribution of the values in our measurements.

The dielectric anisotropy ϵ_a was measured as described in Sec. II B, with the results being shown in Fig. 8(a). ϵ_a remains constant for solutions with block copolymer mass concentrations up to 4%. For the homopolymer solutions, the dielectric anisotropy is slightly larger by about 0.8 compared to the block copolymer solution. Using Eqs. (16) and (17), the splay elastic constant k_{11} and the rotational viscosity γ_1 have been calculated for all samples. The results are shown in Figs. 8(b) and 8(c). The results for γ_1 are also listed in Table I. Obviously, the splay elastic constant k_{11} of the system remains essentially the same over this concentration range. On the other hand, the rotational viscosity increases rapidly with increasing block copolymer concentration, but less pronounced for the homopolymer solutions. For pure 5CB, we measured the values $\epsilon_a = 11$, $k_{11} = 5.3 \times 10^{-12}$ N and $\gamma_1 = 0.08$ Pa s, which are comparable with the literature data [41,42].

TABLE I. Measured rotational viscosity γ_1 with the corresponding standard deviation 2σ for all polymer samples. For pure 5CB, we found $\gamma_1 = 0.078$ Pa s with $2\sigma = 0.010$ Pa s.

	Block copolymer			Homopolymer	
c (%)	γ_1 (Pa s)	2σ (Pa s)	c (%)	γ_1 (Pa s)	2σ (Pa s)
0.2	0.081	0.011	0.5	0.114	0.025
0.5	0.10	0.02	1.0	0.17	0.05
0.8	0.16	0.03	1.5	0.37	0.09
1.1	0.23	0.07	2.0	0.49	0.07
1.3	0.51	0.15	2.5	0.81	0.23
1.5	0.73	0.15			
1.8	2.4	1.3			
2.1	11	3.8			
2.3	47	38			

V. DISCUSSION AND INTERPRETATION

We have found that the cells with mesogenic side-chain block copolymer and homopolymer solutions in 5CB with mass concentrations c up to 2.5% are well aligned and behave like usual nematics. The anisotropy of the dielectric permittivity ϵ_a and the splay elastic constant k_{11} of the solutions do not exhibit any pronounced dependence on concentration within the accuracy of the measurements [see Figs. 8(a) and 8(b)]. Note that for solutions of a different side-chain polymer in 5CB, which do not demonstrate a gel state at high concentrations similar to our homopolymer solutions, the bend elastic constant k_{33} was also found to be independent of the polymer concentration [18]. Nevertheless, the large scatter of the values of k_{11} for the block copolymer solutions especially at higher concentrations already indicates that their elastic properties can be very different from the corresponding homopolymer solutions.

Compared to the elastic properties, the dynamic response characterized by the rotational viscosity γ_1 was found to be much more influenced by the addition of the polymer: γ_1 is increased by a factor of about 500 for a block copolymer concentration of $c = 2.3\%$ and by a factor of about 10 for a homopolymer concentration of $c = 2.5\%$. For concentrations below 1%, the rotational viscosities γ_1^c and γ_1^h for the block copolymer and for the homopolymer, respectively, are increased with c and their values are almost the same. We conclude that the presence of short end blocks in the block copolymer chains in comparison with the homopolymer chains does not influence the rotational viscosity of the solution at low concentrations.

Our most intriguing result is a different concentration dependence of γ_1^c and γ_1^h for solutions with $c > 1\%$, where γ_1^c starts to increase sharply [see Fig. 8(c)]. Note, that, according to rheological measurements and observations in the block copolymer solutions, a fully gelified state is formed for concentrations above $c \approx 3\%$. As already mentioned in Sec. II A, at such concentrations of the ABA-triblock copolymer with polystyrene end blocks (A) and a long middle block (B) with attached mesogenes, a physical network (physical gel) is formed due to the end block interactions [9]. In the nematic phase of 5CB, the end blocks are aggregated in micelles leading to "junctions" between the individual block copolymer chains. The homopolymer does not have the polysterene end blocks and its solutions do not demonstrate the formation of a network.

The increase of the rotational viscosity with concentration can be interpreted in the framework of the Brochard theory for the dynamics of polymer chains in a nematic solvent [15]. This model has been developed for diluted polymer solutions where the polymer chains can be considered as independent, neglecting any interactions between them. The increase of the rotational viscosity $\delta\gamma_1 = \gamma_1(c) - \gamma_1(0)$ with the polymer concentration is given by [15]

$$\delta\gamma_1 = \frac{c_m}{N} k_B T \, \tau_R \, \frac{[1 - (R_\parallel/R_\perp)^2]^2}{(R_\parallel/R_\perp)^2}. \tag{20}$$

Here, c_m is the monomer concentration (the number of monomers per unit volume) and directly proportional to the polymer concentration, N is the degree of polymerization, k_B is the Boltzmann constant, T is the temperature, τ_R is the rotational relaxation time of the polymer chain, and $R_\parallel$, $R_\perp$ are the chain dimensions parallel and perpendicular to the director, respectively, which characterize the anisotropy of the chain shape (aspect ratio). Note that, in the case of an isotropic chain shape ($R_\parallel = R_\perp$), the rotational viscosity of the polymer solution is independent of the polymer concentration. This is in distinct contrast to "hydrodynamic" viscosities (Miesowicz coefficients) determined from shear flow experiments, where the coefficients are proportional to the polymer concentration for any chain shape [14,15]. It has been shown that, for the case of $R_\parallel \approx R_\perp$, a modification of the Brochard theory by including an additional coupling between the side-chain mesogens of the side-chain liquid crystalline polymers with the nematic solvent leads to an improved agreement with experiments [19,20].

The rotational relaxation time of the polymer chain, τ_R, is given as a combination of two relaxation times associated with motions of the chain parallel and perpendicular to the director

$$\tau_R = \tau_\perp \frac{\tau_\parallel/\tau_\perp}{1 + \tau_\parallel/\tau_\perp}, \tag{21}$$

with

$$\tau_\parallel = \frac{\lambda_\parallel}{k_B T} R_\parallel^2, \quad \tau_\perp = \frac{\lambda_\perp}{k_B T} R_\perp^2. \tag{22}$$

Here, $\lambda_\parallel$, $\lambda_\perp$ are the friction coefficients of the polymer chain parallel and perpendicular to the director, respectively. There are two limiting cases for $\lambda_\parallel$ and $\lambda_\perp$ [15,43]. In the free draining limit (a flexible chain freely penetrable by the solvent), one has

$$\lambda_\parallel = N z_\parallel, \quad \lambda_\perp = N z_\perp, \tag{23}$$

where $z_\parallel$ and $z_\perp$ are the monomer friction coefficients in the directions parallel and perpendicular to the director, respectively. In the nondraining limit, corresponding to the approximation of a polymer chain by a rigid sphere impenetrable by the solvent, the friction coefficients are given by

$$\lambda_\parallel \propto R_\parallel, \quad \lambda_\perp \propto R_\perp. \tag{24}$$

To summarize, the rotational viscosity increases linearly with the concentration for polymer chains of anisotropic shape

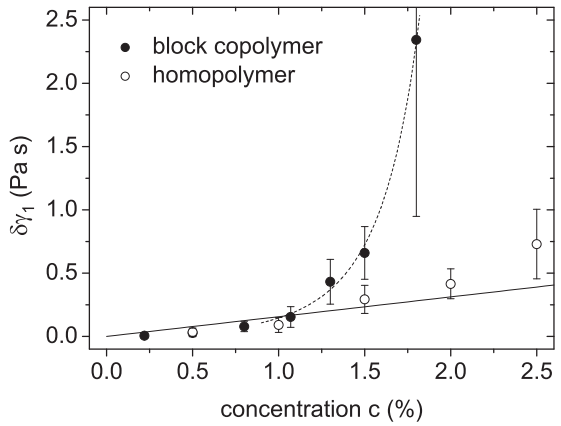

FIG. 9. Increase of the rotational viscosity for the homopolymer ($\delta\gamma_1^h$) and for the block copolymer ($\delta\gamma_1^c$) solutions. The solid line is a linear fit with $\delta\gamma_1^h = 0.156\,c$, while the dashed line is a guide to the eye.

($R_\parallel/R_\perp \neq 1$) and $\delta\gamma_1$ depends on the four microscopic parameters $R_\parallel$, $R_\perp$, $\lambda_\parallel$, and $\lambda_\perp$. The experimental determination of these parameters is a highly complicated task.

Our results for $\delta\gamma_1(c)$ are shown in Fig. 9. We have found that, for the homopolymer solutions, $\delta\gamma_1^h$ increases almost linearly with concentration for $c < 2\%$. Using the coefficient obtained from a linear fit of $\delta\gamma_1^h$, the rotational relaxation time of the homopolymer chain τ_R can be estimated from Eq. (20). Assuming that the density of the solution is approximately equal to the density ρ of pure 5CB, which should be valid for small concentrations, one has $c_m/N = c\rho N_A/M_n$, where N_A is the Avogadro constant and M_n is the molecular mass of the homopolymer. Taking for the geometrical factor in Eq. (20) the value $[1-(R_\parallel/R_\perp)^2]^2/(R_\parallel/R_\perp)^2 \approx 1$, which corresponds to $R_\parallel/R_\perp \approx 0.6$ as found in Ref. [12], we find $\tau_R \approx 0.01$ s. For higher concentrations, $\delta\gamma_1^h$ starts to deviate from the predictions of the Brochard theory. Unfortunately, a theory for the next order corrections ($\propto c^2$) is unavailable at present.

For $c < 1\%$, the increase of the rotational viscosity of the block copolymer solutions is almost the same as for the homopolymer solutions, while for $c > 1\%$, $\delta\gamma_1^c$ starts to increase much more rapidly than $\delta\gamma_1^h$. We suggest that such a sharp increase of $\delta\gamma_1^c$ compared to $\delta\gamma_1^h$ can be related to the formation and growth of larger chains or clusters consisting of individual block copolymer chains attached through the end blocks. The resulting increase of the effective size of the polymer chains can lead to an additional increase of $\delta\gamma_1^c$, taking into account that in Eq. (20) the "effective" degree of polymerization in a block copolymer solution depends on the concentration. As it was shown in Refs. [9,21], side-chain polymers with a sufficiently large degree of polymerization form an oblate configuration and the aspect ratio $R_\parallel/R_\perp < 1$ is independent of N. Therefore, both $R_\parallel$ and $R_\perp$ scale with N in a similar way:

$$R_\parallel \propto N^\beta, \quad R_\perp \propto N^\beta, \tag{25}$$

where the value of the exponent β can vary between $1/3$ for a bad solvent and $3/5$ for a good solvent.

For block copolymer concentrations not too close to the gel point, we assume that preferably free end blocks will join, so that the evolving clusters take the form of almost linear chains without side branches. In this case, the ratio $R_\parallel/R_\perp$ can be regarded as independent of N, as in the case of side-chain polymers with a large degree of polymerization [9,21]. In other words, we assume that a cluster assembled of multiple chains behaves just like one long chain. According to Eqs. (22)–(25), the ratio $\tau_\parallel/\tau_\perp$ can also be considered as independent of N. In addition, the aspect ratios $R_\parallel/R_\perp$ for the block copolymer and for the homopolymer should be the same due to the almost identical chemical structure. Thus, the ratio $\delta\gamma_1^c/\delta\gamma_1^h$ of the change of the rotational viscosity of the block copolymer and the homopolymer solutions can be expressed in terms of the ratio $R_\perp^c/R_\perp^h = R_\parallel^c/R_\parallel^h$ of the chain dimensions. In the following, we use $R_\perp^c/R_\perp^h$ because, in our case, $R_\perp > R_\parallel$. All other microscopic parameters related to the monomers are canceled out since they are identical for both the block copolymer and the homopolymer, and we find

$$\frac{\delta\gamma_1^c}{\delta\gamma_1^h} = \left(\frac{R_\perp^c}{R_\perp^h}\right)^{2+\alpha-1/\beta}, \tag{26}$$

where $\alpha = 1/\beta$ corresponds to the free draining limit [see Eq. (23)] and $\alpha = 1$ to the nondraining limit [see Eq. (24)]. Thus, the increase of the ratio $\delta\gamma_1^c/\delta\gamma_1^h$ with concentration yields a measure for the effective size of the attached block copolymer chains in units of a single chain size. This relation is still valid when taking into account the correction to the Brochard model as proposed in Ref. [19].

The fully gelified state of the block copolymer solution occurs above $c \approx 3\%$. Below this point, the value of $R_\perp^c/R_\perp^h$ should obey a scaling law [44,45]

$$\frac{R_\perp^c}{R_\perp^h} \propto (c_{\rm gel} - c)^{-\nu}, \tag{27}$$

where $c_{\rm gel}$ is the critical concentration when the fraction of the solution is equal to the fraction of the gel (sol-gel transition) and ν is the critical exponent. Although the exponent ν in Eq. (27) can hardly be related to the appropriate critical exponents that appear in various models of percolation theory of chemical gels [1,44,45], the scaling behavior should nevertheless hold.

Using Eqs. (26) and (27), we fitted the experimental ratio $\delta\gamma_1^c/\delta\gamma_1^h$ as

$$\frac{\delta\gamma_1^c}{\delta\gamma_1^h} = a(c_{\rm gel} - c)^{-b}. \tag{28}$$

For the data of $\delta\gamma_1^c(c)$ at a given c, interpolated values of $\delta\gamma_1^h$ were used to find the desired ratio. Our results as a function of the block copolymer concentration are shown in Fig. 10 together with the fit. From the fitting procedure, we find

$$c_{\rm gel} = 2.7\% \quad \text{and} \quad b = \nu(2+\alpha-1/\beta) = 3.45. \tag{29}$$

Up to now, no assumption has been made on the draining behavior and on the solubility of the polymer chains in the solvent.

Since the mesogenic side-chain moieties of the block copolymer are structurally similar to 5CB, and the middle block is soluble in the nematic phase as well as in the isotropic phase of 5CB, it is quite reasonable to suggest that we are dealing with flexible polymer chains in a good solvent. Then,

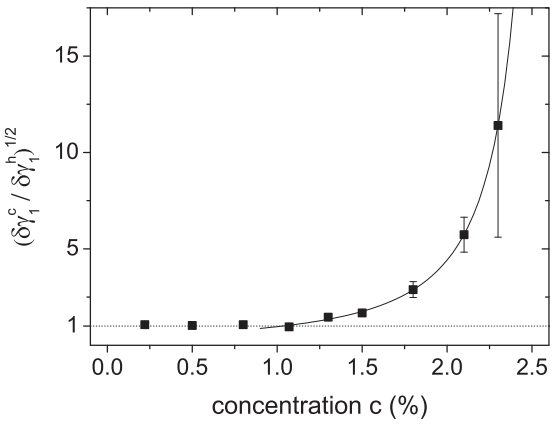

FIG. 10. Dependence of $(\delta\gamma_1^c/\delta\gamma_1^h)^{1/2}$ and, thus, $R_\perp^c/R_\perp^h$ on the block copolymer concentration c. The solid line is obtained by fitting Eq. (28) to the data above $c = 1\%$.

the properties of such chains should be close to the free draining limiting case where $\alpha = 1/\beta$. This yields $\nu = 1.7$ for the critical exponent. The values of $(\delta\gamma_1^c/\delta\gamma_1^h)^{1/2}$ should then give the measure for the effective size of the attached block copolymer chains in units of a single chain size $R_\perp^c/R_\perp^h$ [see Eq. (26) for $\alpha = 1/\beta$]. The values of $(\delta\gamma_1^c/\delta\gamma_1^h)^{1/2} = R_\perp^c/R_\perp^h$ look quite plausible, indicating that, for $c > 1\%$, the block copolymer chains start to join and the effective size of the chains increases by up to 10 individual chain sizes at the highest concentration that has been studied.

Most importantly, the value for the critical concentration $c_{\text{gel}} = 2.7\%$ for the sol-gel transition obtained from Eq. (28) is independent of the chain model and is very close to the concentration $c \approx 3\%$, above which the fully gelified state was identified from rheological measurements [35]. Note that the value of c_{gel} obtained from fitting the experimental data by Eq. (28) is less sensitive to the accuracy of the measurements of $\delta\gamma_1^c$, $\delta\gamma_1^h$ than the value of b. Thus, the scaling behavior of the rotational viscosity can be useful to determine the critical concentration for the sol-gel transition.

VI. SUMMARY AND CONCLUSION

We found that, for the homopolymer solutions, which do not form a gel state, the splay elastic constant k_{11} remains constant. In the case of the block copolymer solutions, we found a large scatter of k_{11} when approaching the gel point, so that we can not assert unambiguously that the elasticity changes. However, the coupling between the reorientation of the director and the elastic deformations of the polymer network clusters can lead to an effective renormalization of the elastic properties of the solution. The characterization of the interplay between the elastic properties of the polymer network and the nematic liquid crystal in the fully gelified state is a key question for the application of various theoretical models to liquid crystalline gels [46,47]. Thus, more accurate measurements of the dependencies of all three elastic constants on the polymer concentration could be useful to identify the anisotropy of the interactions between the liquid crystal and the network clusters forming near the gel point.

The most significant difference in the behavior of the block copolymer and the homopolymer solutions has been found in their dynamical properties characterized by the rotational viscosity γ_1. For small concentrations $c < 1\%$, the rotational viscosities of both solutions increase with c and are almost equal to each other. For larger concentrations $c > 1\%$, however, the rotational viscosity of the block copolymer solutions sharply increases and tends to diverge, while γ_1 for the homopolymer solutions exhibits an almost linear dependence on c. Comparing the results obtained for both solutions, we were able to attribute the critical scaling-law behavior of the rotational viscosity of the block copolymer solutions with the formation of network clusters when approaching the gel point. The critical concentration of the block copolymer for the sol-gel transition obtained from the rotational viscosity data is very close to the value found from rheological measurements. Thus, the dynamic Fréedericksz transition technique can serve as an alternative approach for the determination of the critical concentration and has apparent advantages in comparison with rheological and dynamic light scattering measurements. We have also estimated the dependence of the effective cluster size on the block copolymer concentration. In principle, combining these results with the measurements of the flow-alignment angle or the Miesowicz viscosities would allow us to determine in addition the shape anisotropy of the clusters. The information about the cluster size growth with polymer concentration and their shape anisotropy is of great importance to understand the structure of the network formed in the gel state, and also to validate the relevant models for the sol-gel transition.

ACKNOWLEDGMENTS

We gratefully acknowledge the financial support of the Deutsche Forschungsgemeinschaft (DFG), FOR608, project "Thermoreversible liquid crystalline gels under the influence of electric fields". One of us (M.Kh.) wishes to thank the University of Bayreuth for its kind hospitality.

[1] J. E. Martin and D. Adolf, Annu. Rev. Phys. Chem. **42**, 311 (1991).
[2] K. Almdal, J. Dyre, S. Hvidt, and O. Kramer, Polym. Gels Networks **1**, 5 (1993).
[3] P. G. de Gennes and J. Prost, *The Physics of Liquid Crystals* (Clarendon, Oxford, 1993).
[4] T. Kato, Y. Hirai, S. Nakaso, and M. Moriyama, Chem. Soc. Rev. **36**, 1857 (2007).
[5] K. Urayama, Macromolecules **40**, 2277 (2007).
[6] R. Zentel, Liq. Cryst. **1**, 589 (1986).
[7] Y. Yusuf, J. H. Huh, P. E. Cladis, H. R. Brand, H. Finkelmann, and S. Kai, Phys. Rev. E **71**, 061702 (2005).
[8] R. Pelrine, R. Kornbluh, Q. Pei, and J. Joseph, Science **287**, 836 (2000).
[9] M. D. Kempe, N. R. Scruggs, R. Verduzco, J. Lal, and J. A. Kornfield, Nat. Mater. **3**, 177 (2004).

[10] K. Kajiwara, S. Kohjiya, M. Shibayama, and H. Urakawa, in *Polymer Gels*, edited by D. DeRossi, K. Kajiwara, Y. Osada, and A. Yamauchi (Plenum Press, New York, 1991), p. 3.
[11] M. H. Li, P. Keller, J. Yang, and P. A. Albouy, Adv. Mater. **16**, 1922 (2004).
[12] M. D. Kempe, R. Verduzco, N. R. Scruggs, and J. A. Kornfield, Soft Matter **2**, 422 (2006).
[13] R. Verduzco, N. R. Scruggs, S. Sprunt, P. Palffy-Muhoray, and J. A. Kornfield, Soft Matter **3**, 993 (2007).
[14] A. Jamieson, Prog. Polym. Sci. **21**, 981 (1996).
[15] F. Brochard, J. Polym. Sci., Polym. Phys. Ed. **17**, 1367 (1979).
[16] X. J. Wang and M. Warner, J. Phys. A: Math Gen. **20**, 713 (1987).
[17] A. Matsuyama and Y. Kushibe, J. Chem. Phys. **132**, 104903 (2010).
[18] E. E. Pashkovsky and T. G. Litvina, Macromolecules **28**, 1818 (1995).
[19] N. Yao and A. M. Jamieson, Macromolecules **31**, 5399 (1998).
[20] P.-Y. Liu, N. Yao, and A. M. Jamieson, Macromolecules **32**, 6587 (1999).
[21] M. D. Kempe, J. A. Kornfield, and J. Lal, Macromolecules **37**, 8730 (2004).
[22] D. F. Gu and A. M. Jamieson, Macromolecules **27**, 337 (1994).
[23] M. D. Kempe and J. A. Kornfield, Phys. Rev. Lett. **90**, 115501 (2003).
[24] P. Pieranski, F. Brochard, and E. Guyon, Le J. de Phys. **33**, 681 (1972).
[25] P. Pieranski, F. Brochard, and E. Guyon, Le J. de Phys. **34**, 35 (1973).
[26] F.-L. Chen, A. M. Jamieson, M. Kawasumi, and V. Percec, J. Polym. Sci., Part B: Polym. Phys. **33**, 1213 (1995).
[27] C. C. Chang, L. C. Chien, and R. B. Meyer, Phys. Rev. E **56**, 595 (1997).
[28] A. de Lózar, W. Schöpf, I. Rehberg, O. Lafuente, and G. Lattermann, Phys. Rev. E **71**, 051707 (2005).
[29] M. Müller, W. Schöpf, I. Rehberg, A. Timme, and G. Lattermann, Phys. Rev. E **76**, 061701 (2007).
[30] J. Adams and W. Gronski, Makromol. Chem., Rapid Commun. **10**, 553 (1989).
[31] G. Mao, J. Wang, S. R. Clingman, C. K. Ober, J. T. Chen, and E. L. Thomas, Macromolecules **30**, 2556 (1997).
[32] C. Frenz, A. Fuchs, H.-W. Schmidt, U. Theissen, and D. Haarer, Macromol. Chem. Phys. **205**, 1246 (2004).
[33] T. Breiner, K. Kreger, R. Hagen, M. Haeckel, L. Kador, A. H. E. Mueller, E. J. Kramer, and H.-W. Schmidt, Macromolecules **40**, 2100 (2007).
[34] See Supplemental Material at http://link.aps.org/supplemental/10.1103/PhysRevE.84.021710 for details regarding the synthesis and characterization of the block copolymer and of the respective homopolymer.
[35] R. Pettau *et al.* (unpublished).
[36] H. Mada and S. Kobayashi, Mol. Cryst. Liq. Cryst. **33**, 47 (1976).
[37] I. Rehberg, B. L. Winkler, M. de la Torre Juárez, S. Rasenat, and W. Schöpf, Adv. Solid State Phys. **29**, 35 (1989).
[38] A. de Lózar, W. Schöpf, I. Rehberg, Ó. Lafuente, and G. Lattermann, Phys. Rev. E **71**, 051707 (2005).
[39] A. Bogi and S. Faetti, Liq. Cryst. **28**, 729 (2001).
[40] S. A. Pikin, *Structural Transformations in Liquid Crystals*, 1st ed. (Gordon and Breach, New York, 1991).
[41] L. M. Blinov and V. G. Chigrinov, *Electrooptic Effects in Liquid Crystal Materials* (Springer, New York, 1994).
[42] G. Ahlers, in *Pattern Formation in Liquid Crystals*, edited by A. Buka and L. Kramer (Springer, New York, 1996), p. 127.
[43] W. Graessley, *Polymeric Liquids & Networks: Dynamics and Rheology* (Garland Science, London, 2008).
[44] D. Stauffer, Phys. Rep. **54**, 1 (1979).
[45] P. G. De Gennes, *Scaling Concepts in Polymer Physics*, 1st ed. (Cornell University Press, Ithaca, NY, 1980).
[46] M. Warner and E. Terentjev, *Liquid Crystal Elastomers* (Oxford University Press, Oxford, 2003).
[47] H. Brand, H. Pleiner, and P. Martinoty, Soft Matter **2**, 182 (2006).